

μ -synthesis-based Generalized Robust Framework for Grid-following and Grid-forming Inverters

Soham Chakraborty, *Student Member, IEEE*, Sourav Patel, *Member, IEEE*, and Murti V. Salapaka, *Fellow, IEEE*

Abstract—Grid-following and grid-forming inverters are integral components of microgrids and for integration of renewable energy sources with the grid. For grid following inverters, which need to emulate controllable current sources, a significant challenge is to address the large uncertainty of the grid impedance. For grid forming inverters, which need to emulate a controllable voltage source, large uncertainty due to varying loads has to be addressed. In this article, a μ -synthesis-based robust control design methodology, where performance under quantified uncertainty is guaranteed, is developed under a unified approach for both grid-following and grid-forming inverters. The control objectives, while designing the proposed optimal controllers, are: i) reference tracking, disturbance rejection, harmonic compensation capability with sufficient LCL resonance damping under large variations of grid impedance uncertainty for grid-following inverters; ii) reference tracking, disturbance rejection, harmonic compensation capability with enhanced dynamic response under large variations of equivalent loading uncertainty for grid-forming inverters. A combined system-in-the-loop (SIL), controller hardware-in-the-loop (CHIL) and power hardware-in-the-loop (PHIL) based experimental validation on 10 kVA microgrid system with two physical inverter systems is conducted in order to evaluate the efficacy and viability of the proposed controllers.

Index Terms—Grid-following inverter, grid-forming inverter, \mathcal{H}_∞ -based loop shaping, parametric uncertainty, robust control.

I. INTRODUCTION

WITH the proliferation of inverter-interfaced distributed energy resources, there is a renewed emphasis on local microgrids that provide operational flexibility and aid sustainability for the energy infrastructures. Both grid-forming (GFM) and grid-following (GFL) inverters have become essential components that have pivotal roles to play in such microgrids operating both in grid-tied and islanded mode. During islanded mode, GFM inverters maintain a stable voltage and frequency of the microgrid in the absence of grid. Whereas, GFL inverters are usually operated to supply power where voltage and frequency are maintained either by the grid or other GFM inverters [1]. In the hierarchical structure of microgrid control system, *inner* voltage-control loops, regulating voltage to specified values, are responsible for GFM inverters to emulate controllable voltage sources. Similarly, GFL inverters emulate controllable current sources by regulating currents via *inner* current-control loop [2].

Typically GFL inverters are connected to grid via LCL filters for high frequency attenuation caused by switching.

S. Chakraborty, S. Patel, M. V. Salapaka are with the Department of Electrical and Computer Engineering, University of Minnesota, Minneapolis, 55455 MN, USA e-mail: chakr138@umn.edu, patel292@umn.edu, murtis@umn.edu

The authors acknowledge Advanced Research Projects Agency-Energy (ARPA-E) for supporting this research through the project titled “Rapidly Viable Sustained Grid” via grant no. DE-AR0001016.

Multiple important factors are considered in the design stage of GFL inverters including 1) resonances caused by low-damping of the LCL filter in GFL inverters, while connected to weak grid, that could lead to system instability. Here, proper damping of such resonance is crucial while designing [3]; 2) Uncertainty in variation of grid impedance parameters significantly influence the robustness of the output current controller. For example, increase in grid inductance requires reduction in the gain and bandwidth of the current controller to keep the system stable that leads to degradation of tracking performance and disturbance rejection capability. Here, there is a need for control design that delivers optimal performance while guaranteeing stability for the range of grid impedance encountered in practice [4]; 3) Grid impedance variation causes variation in resonance frequency of the inverter system that impacts active damping methods. Here, robustness of the active damping to remain effective under uncertainty is required [5]; 4) Most importantly, the controller should result in good tracking performance, disturbance rejection and harmonic compensation capability while remaining implementable in low-cost micro-controllers. Various types of control schemes and their advancements for GFL inverters are proposed in literature [6]. Major current-control schemes for GFL inverters, reported in existing literature, are compared in Fig. 1(a). In summary, existing methods include classical (i.e. proportional/integral/resonant controller-based), hysteresis, sliding-mode, model predictive, repetitive, LQR, \mathcal{H}_∞ -based control schemes as reported in [3]–[24]. Broadly, these schemes use, either passive damping with or without new filter topology or, active damping using either additional measurements for feedforward control action. These additional measurements increase the cost of availing multiple sensors. Moreover, most of the schemes do not provide guaranteed robustness both in active damping and in controller performance under varying and uncertain grid impedance.

Similarly, designing the voltage controller for GFM inverter is essentially a multi-objective task. The design considerations include 1) reference tracking, disturbance rejection and harmonic compensation in presence of various linear and non-linear loads; 2) The voltage controllers are required to provide compensation to dynamic variations of the output load current and improve the dynamic response [25]; 3) Unknown nature of the output loading of GFM inverter can significantly alter the system behavior. Here during heavily loaded condition of GFM inverter, transient performance is severely compromised [26]. Therefore, the voltage controller should be robust enough against unknown loading uncertainties to perform all the aforementioned tasks. Numerous voltage control strategies are proposed in the literature during past decades for GFM inverter system [27]. Major voltage-

Ref.	LCL Damping	Robustness Against Grid Impedance Parameter Variation	Ref.	Improved Dynamic Response	Robustness Against Equivalent Load Parameter Variation
[3] [7]–[15]	<ul style="list-style-type: none"> • New filter topology • Additional feedforward of grid voltage, grid current, inner capacitor current • State feedback control • Lack robust damping 	<ul style="list-style-type: none"> • Lack robustness under varying unknown grid impedance • Designed with known, fixed, nominal grid impedance 	[26] [28]–[30] [31]–[33]	<ul style="list-style-type: none"> • Multiloop control structure • Feedback of inductor current, inner capacitor current • Disturbance observer design • Dominant pole elimination • Need multiple measurements 	<ul style="list-style-type: none"> • Lack robustness during variation of equivalent loading • Designed controller for rated loading condition • No loading uncertainty
[4], [5] [16]–[21] [22]–[24]	<ul style="list-style-type: none"> • Passive damping • Additional outer current inner current loop • Inherent active damping using controller shaping • Challenging during varying grid impedance 	<ul style="list-style-type: none"> • Lack robustness under varying unknown grid impedance • Grid impedance uncertainty not designed for controller synthesis 	[34]–[36] [37]–[40] [41]–[43]	<ul style="list-style-type: none"> • Multiloop control structure with sliding mode, LQR, $\mathcal{H}_2/\mathcal{H}_\infty$, $\mathcal{H}_\infty/\mathcal{H}_\infty$ control • Complicated, loopy structure with multiple measurements • Challenging during varying equivalent loading conditions 	<ul style="list-style-type: none"> • Lack robustness for full range variation of equivalent loading • Lack robust performance • Designed controller for simple load uncertainty, without non-linear load
Proposed	<ul style="list-style-type: none"> ✓ Single loop control leads reduction in measurements ✓ Inherent active damping using controller shaping ✓ Robust damping under varying grid impedance 	<ul style="list-style-type: none"> ✓ Grid impedance uncertainty designed for controller synthesis ✓ Exhibit robustness under varying unknown grid impedance 	Proposed	<ul style="list-style-type: none"> ✓ \mathcal{H}_∞-based robust control ✓ Single loop control structure ✓ No need of feedforward loop ✓ Reduction in measurements ✓ Enhancement of dynamic response by controller shaping 	<ul style="list-style-type: none"> ✓ Equivalent loading uncertainty designed for controller synthesis ✓ Exhibit robustness under the variation of equivalent loading

(a) Major works on grid-following inverter control

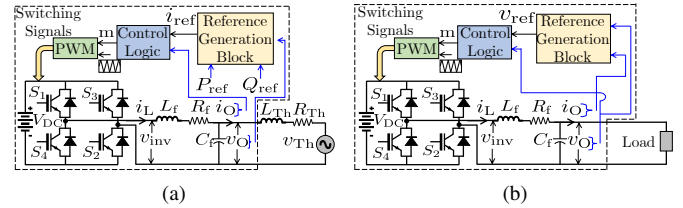
(b) Major works on grid-forming inverter control

Fig. 1. A summary of major current-control and voltage-control strategies for grid-following and grid-forming inverters proposed since last decade respectively.

control schemes, reported in existing literature, are shown in Fig. 1(b). In summary, there are nested-loop classical (i.e. proportional/integral/resonant controller-based), sliding-mode, model predictive, repetitive, LQR, \mathcal{H}_∞ -based, \mathcal{H}_2 -based control schemes as reported in [26]–[43]. Most of the advancements have focused on either multiple nested-loop structures with advanced control techniques or adding extra measurements as feedforward for enhancing dynamic performance. This results in either increased complication of the control structure that lead to difficulties in implementation or increase in the capital cost for availing multiple sensors. Also, most of the schemes face deteriorating dynamic response and lack robustness in controller performance under varying and uncertain equivalent loading.

This article presents a generalized μ -synthesis-based robust control framework and leverages a voltage-current duality in the plant dynamic model of GFL and GFM inverters. By modeling and quantifying the uncertainties in grid impedance parameters and uncertainties in equivalent loading parameters for GFL and GFM inverters respectively, the generalized control framework results in controllers that are single-loop, hence simple and cost-effective. The resulting controllers offer ease of implementation and provide optimal robustness in performance under uncertainties with respect to good reference tracking, disturbance rejection and harmonic compensation capabilities. Moreover, the resulting current-controller for GFL inverter provides inherent active damping under grid parameter variation and the resulting voltage-controller for GFM inverter enhances the dynamic performance during load transients. A combined system-in-the-loop (SIL), controller-hardware-in-the-loop (CHIL) and power-hardware-in-the-loop (PHIL) - based experiment is conducted to evaluate the efficacy and viability of the proposed controllers.

This article is organized as follows. In Section II, the problem formulation and motivation of the study are presented. In Section III, the proposed generalized μ -synthesis-based robust control framework is described. Section IV provides the controller synthesis and corresponding stability analysis. In Section V, the experimental setup and corresponding results are described. Finally, Section VI concludes the paper.

Fig. 2. A 1- ϕ (a) grid-following inverter, and (b) grid-forming inverter.

II. PROBLEM FORMULATION AND MOTIVATION

In this section control problem formulation will be discussed for inverter system operating in GFL and GFM mode. For both GFL and GFM inverters, a single-phase H-bridge inverter is considered comprising a dc bus, V_{DC} , four switching devices, S_1, S_2, S_3, S_4 , and an LCL filter with L_f, L_g, R_f, R_g and C_f as inverter and grid side filter inductors, parasitic resistances and filter capacitor respectively. A control layer is employed with sinusoidal PWM switching technique to generate the switching signals for power circuit.

A. Problem Formulation for Grid-following Inverter

A GFL inverter is connected to a distribution grid, represented by the Thevenin equivalent voltage source, v_{Th} , in series with the Thevenin equivalent impedance, $Z_{Th} := R_{Th} + j\omega_o L_{Th}$. ω_o (in rad/sec) is the frequency of the distribution network. For simplicity, the Thevenin equivalent impedance accounts grid side filter parameters also (i.e. L_g, R_g). Various components of GFL inverter system are shown in Fig. 2(a). In this operation, the inverter operates with an output current control strategy to regulate real and reactive power output where the voltage and frequency of the distribution network are determined by another source such as the grid or other GFM inverters. The goal of the current controller is to generate a controlled voltage signal, v_{inv} , by switching signals such that the output current, i_O , tracks the reference signal,

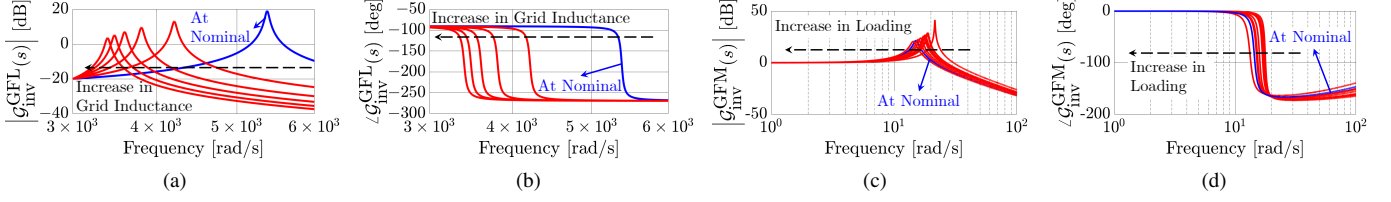


Fig. 3. Bode plots of (a) magnitude and (b) phase of $\mathcal{G}_{inv}^{GFL}(s)$ of (4) and (c) magnitude and (d) phase of $\mathcal{G}_{inv}^{GFM}(s)$ of (13) respectively.

i_{ref} , generated by reference generation block as discussed in Appendix A. The dynamics of the inverter are described as:

$$L_f \frac{d\langle i_L \rangle}{dt} + R_f \langle i_L \rangle = \langle v_{inv} \rangle - \langle v_O \rangle, \quad (1)$$

$$L_{Th} \frac{d\langle i_O \rangle}{dt} + R_{Th} \langle i_O \rangle = \langle v_O \rangle - \langle v_{Th} \rangle, \quad (2)$$

$$C_f \frac{d\langle v_O \rangle}{dt} = \langle i_L \rangle - \langle i_O \rangle, \quad (3)$$

where $\langle \cdot \rangle$ signifies the average values of the corresponding variable over one switching cycle (T_s) [25]. Laplace transformation and algebraic manipulation with (1), (2) and (3) result:

$$i_O(s) = \mathcal{G}_{inv}^{GFL}(s)v_{inv}(s) - \mathcal{G}_{Th}^{GFL}(s)v_{Th}(s), \quad (4)$$

where, $\mathcal{G}_{inv}^{GFL}(s)$ and $\mathcal{G}_{Th}^{GFL}(s)$ are transfer functions parameterized by L_f , R_f , C_f , L_{Th} and R_{Th} , as given in (5) and (6). As observed in (4), distribution network has two-fold impacts on the open-loop plant dynamics. $v_{Th}(s)$ acts as an exogenous disturbance signal to the plant which can be addressed by classical disturbance rejection problem. Both $\mathcal{G}_{inv}^{GFL}(s)$ and $\mathcal{G}_{Th}^{GFL}(s)$ consist of L_{Th} and R_{Th} as parameters. Variation of these parameters due to changing distribution network topology introduces uncertainties in the plant model [23], [24]. Fig. 3(a) and Fig. 3(b) show the Bode plot of $\mathcal{G}_{inv}^{GFL}(s)$ that clearly shows the large variation in frequency response of the open-loop plant model due to grid inductance variation. Fig. 3(a) shows that the equivalent LCL resonant peak is sensitive to grid inductance, L_{Th} . For stiff grid with small L_{Th} (leading to a large resonant frequency), the resultant resonant frequency is larger than the bandwidth of the controller. However, such a controller when used for a sufficiently weak grid with large L_{Th} , the resultant resonance peak may enter the pass-band of the current controller that in turn results in instability [23], [24]. As a result, this uncertainty in grid impedance parameters introduces challenges with respect to performance under uncertainty of grid impedance. With this motivation, this article designs a single-loop μ -synthesis-based stabilizing controller for GFL inverter that has robust active damping, tracking performance, disturbance rejection and harmonic compensation under grid impedance uncertainties.

B. Problem Formulation for Grid-forming Inverter

Various components of a GFM inverter are shown in Fig. 2(b). A GFM inverter is connected across an equivalent load that represents the corresponding loading of the inverter while connected to any network. For simplicity, the grid side filter parameters are also included in the equivalent loading. In this mode, the inverter operates with an output voltage control strategy to generate a stable voltage and frequency across the equivalent load. The goal of the voltage control logic is to generate a controlled voltage signal, v_{inv} , by switching signals such that the output voltage, v_O , tracks the reference signal, v_{ref} , generated by reference generation layer as discussed in Appendix B. The dynamics of the inverter are described as:

$$L_f \frac{d\langle i_L \rangle}{dt} + R_f \langle i_L \rangle = \langle v_{inv} \rangle - \langle v_O \rangle, \quad (7)$$

$$C_f \frac{d\langle v_O \rangle}{dt} = \langle i_L \rangle - \langle i_O \rangle, \quad (8)$$

where $\langle \cdot \rangle$ signifies the average values of the corresponding variable over one switching cycle (T_s) [25]. Laplace transformation and algebraic manipulation with (7) and (8) result:

$$v_O(s) = \mathcal{G}_1(s)v_{inv}(s) - \mathcal{G}_2(s)i_O(s), \quad (9)$$

where, $\mathcal{G}_1(s)$ and $\mathcal{G}_2(s)$ are transfer functions parameterized by L_f , R_f , C_f , as given in (10) and (11) and described by:

$$\mathcal{G}_1(s) = \frac{1}{[L_f C_f]s^2 + [R_f C_f]s + 1} \quad \text{and} \quad (10)$$

$$\mathcal{G}_2(s) = \frac{L_f s + R_f}{[L_f C_f]s^2 + [R_f C_f]s + 1}. \quad (11)$$

The nature of the equivalent load is essential for characterizing i_O . In this work, the equivalent load is modeled by a parallel combination of two components. First component is a linear admittance, $Y_{Load}(s) := 1/(L_{Load}s + R_{Load})$, with unknown R_{Load} and L_{Load} elements in series combination; the grid side filter parameters are included in R_{Load} and L_{Load} . Another component is a parallel combination of current sources consisting of both fundamental and harmonic components [44] and defined as: $i_h(s) := \sum_k i_k(s)$, where k is odd and $i_k(s)$ is k^{th} harmonic current. As a result, $i_O(s)$ is characterized as:

$$i_O(s) = Y_{Load}(s)v_O(s) + i_h(s). \quad (12)$$

$$\mathcal{G}_{inv}^{GFL}(s) = 1/[(C_f L_f L_{Th})s^3 + C_f(L_{Th} R_f + L_f R_{Th})s^2 + (C_f R_f R_{Th} + L_f + L_{Th})s + (R_f + R_{Th})] \quad (5)$$

$$\mathcal{G}_{Th}^{GFL}(s) = [(C_f L_f)s^2 + (C_f R_f)s + 1]\mathcal{G}_{inv}^{GFL}(s) \quad (6)$$

Combining (9) and (12), system's dynamic equation becomes:

$$v_O(s) = \mathcal{G}_{inv}^{GFM}(s)v_{inv}(s) - \mathcal{G}_{Load}^{GFM}(s)i_h(s), \quad (13)$$

where, $\mathcal{G}_{inv}^{GFM}(s)$ and $\mathcal{G}_{Load}^{GFM}(s)$ are transfer functions parameterized by L_f , R_f , C_f , L_{Load} and R_{Load} , as given in (14) and (15). As observed in (13), load has impacts on the open-loop plant dynamics of the GFM inverter. Firstly, both $\mathcal{G}_{inv}^{GFM}(s)$ and $\mathcal{G}_{Load}^{GFM}(s)$ consist of L_{Load} and R_{Load} as parameters. that introduce uncertainties in the plant model. Variation of these parameters due to loading of the inverter due to changing generation-load imbalance in the distribution network introduces uncertainties in the plant model [34], [35]. Secondly, $i_h(s)$, imposed by the fundamental and harmonic current load, acts as an exogenous disturbance signal to the plant. Where the latter one is a classical disturbance rejection problem, the former one poses robustness issues. Fig. 3(c) and Fig. 3(d) depict the Bode plot of $\mathcal{G}_{inv}^{GFM}(s)$ that shows the variation in frequency response of the open-loop plant model due to variation in equivalent loading. It is also evident that the uncertain loading variation across the inverter causes significant change in the plant dynamics, especially the effective resonant frequency of the inverter system as shown in Fig. 3(c). This deteriorates the transient response of the GFM inverter severely as well as overall system stability [26], [37]. with the above motivation, this article designs a single-loop μ -synthesis-based stabilizing controller that has robust tracking performance, disturbance rejection and harmonic compensation with improved transient operation under the full range variation in equivalent loading.

III. μ -SYNTHESIS-BASED GENERALIZED FRAMEWORK FOR CONTROLLER SYNTHESIS

Motivated by Section II-A and II-B, this section will describe the generalized control framework and required modeling for μ -synthesis-based controller synthesis.

A. μ -synthesis-based Generalized Framework

The following observations are common for both GFL and GFM inverter system:

I) The open-loop plant model, $\mathcal{G}_{inv}^{GFL}(s)$ of (5) and $\mathcal{G}_{inv}^{GFM}(s)$ of (14) are 3rd order model with difference numerator type for GFL and GFM inverter respectively. Whereas the disturbance model, $\mathcal{G}_{Th}^{GFL}(s)$ of (6) and $\mathcal{G}_{Load}^{GFM}(s)$ of (15), are 3rd order models for GFL and GFM respectively. Moreover, there is a voltage-current duality in the plant dynamic model of GFL and GFM inverter. Here for both the models, v_{inv} is the *plant input* signal, i_O , v_O are the *plant output* and v_{Th} , i_h are the *disturbance* signal for GFL and GFM inverter respectively as given in (4) and (13).

II) The open-loop plant and disturbance models have similar parametric uncertainties imposed by L_{Th} , R_{Th} and L_{Load} and R_{Load} for both GFL and GFM inverter respectively. The similarity is evident in Fig. 4 and Fig. 5 where the open-loop

plant models are shown using block diagram inside the blue boxes and corresponding uncertainty block using dashed ovals for both GFL and GFM inverter respectively.

III) Robust tracking performance, disturbance rejection and harmonic compensation capabilities are desired for controllers of GFL and GFM inverters under the uncertainties.

Item **I)** and **II)** motivate designing a generalized control framework for GFL and GFM inverters based on these similarity and duality property. Third point warrants the μ -synthesis-based robust controller synthesis for addressing multiple objectives. A systematic approach is presented below for designing controller, $\mathcal{C}_{H\infty}(s)$ of Fig. 4 and Fig. 5 for GFL and GFM inverter respectively using the generalized μ -synthesis-based robust control framework.

B. Modeling of Uncertainty

It can be observed that in both the GFL and GFM inverter open-loop plant model, the model uncertainty is present as parametric uncertainties in 1st order transfer function (dashed ovals in Fig. 4 and Fig. 5 respectively). A systematic approach is followed here for characterizing and modeling the uncertainty for both the cases as discussed below:

1) Characterizing the Uncertainty for GFL Inverter: Variations in grid impedance (i.e. L_{Th} and R_{Th}) results in real-parametric uncertainties in the GFL plant model. The short-circuit ratio (SCR) is often used to characterize the grid stiffness and can be employed in determining the Thevenin equivalent impedance of the grid at the point-of-connection. SCR is defined as $(V_{PC}^N)^2 / [S_B \sqrt{(\omega_N L_{Th})^2 + R_{Th}^2}]$, where V_{PC}^N and ω_N are the nominal voltage and frequency at point-of-connection, and S_B is the rated apparent power of the GFL inverter. Usually the grid at point-of-connection is considered as weak when the SCR is less than 3 [44], [45]. In this work, with a pre-specified SCR (< 3) and X/R ratio (< 10), the nominal grid impedance parameters, denoted as L_{Th}^{Nom} and R_{Th}^{Nom} , are determined. By considering $\pm 100\%$ variations over nominal values, it is assumed that $L_{Th} \in [\underline{L}_{Th}, \bar{L}_{Th}]$ and $R_{Th} \in [\underline{R}_{Th}, \bar{R}_{Th}]$. It is to be noted that very stiff to extremely weak grid conditions are accommodated with this uncertainty characterization. As a result,

$$L_{Th} := L_{Th}^{Nom} + w_{Th}^L \delta_L, \quad R_{Th} := R_{Th}^{Nom} + w_{Th}^R \delta_R, \quad (16)$$

where, $\delta_L, \delta_R \in [-1, 1]$, $L_{Th}^{Nom} = \frac{1}{2}[\bar{L}_{Th} + \underline{L}_{Th}]$, $R_{Th}^{Nom} = \frac{1}{2}[\bar{R}_{Th} + \underline{R}_{Th}]$, $w_{Th}^L = \frac{1}{2}[\bar{L}_{Th} - \underline{L}_{Th}]$, $w_{Th}^R = \frac{1}{2}[\bar{R}_{Th} - \underline{R}_{Th}]$.

2) Characterizing the Uncertainty for GFM Inverter: In this case, variation in equivalent loading (i.e. R_{Load} and L_{Load}) results in real-parametric uncertainties in the GFM plant model. In this work, the linear part of the loading is modeled by a series combination of equivalent unknown R_{Load} and L_{Load} element. These elements are at nominal while the GFM inverter loading is at rated condition. Considering rated

$$\mathcal{G}_{inv}^{GFM}(s) = [L_{Load}s + R_{Load}] / [(C_f L_f L_{Load})s^3 + C_f (L_{Load} R_f + L_f R_{Load})s^2 + (C_f R_f R_{Load} + L_f + L_{Load})s + (R_f + R_{Load})] \quad (14)$$

$$\mathcal{G}_{Load}^{GFM}(s) = \mathcal{G}_{inv}^{GFM}(s) [(L_{Load} L_f)s^2 + (L_{Load} R_f + L_f R_{Load})s + (R_{Load} R_f)] / [L_{Load}s + R_{Load}] \quad (15)$$

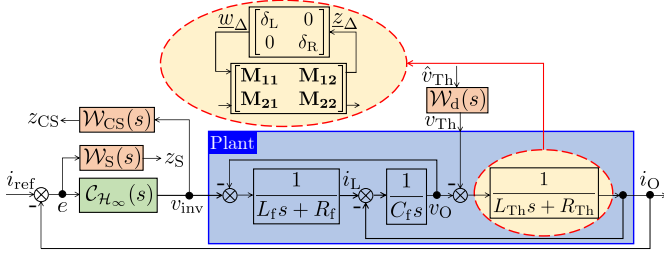


Fig. 4. Proposed μ -synthesis-based robust controller for GFL Inverter.

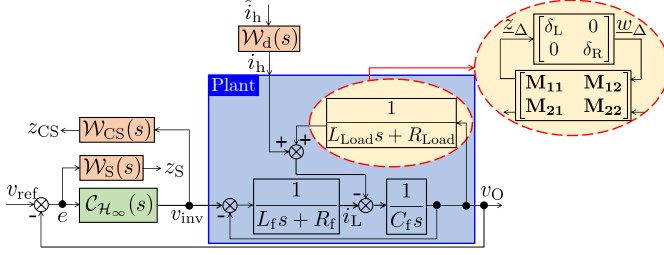


Fig. 5. Proposed μ -synthesis-based robust controller for GFM Inverter.

VA loading as S_{rated} , with active power, P_{rated} , and reactive power, Q_{rated} , the following holds for nominal values:

$$R_{\text{Load}}^{\text{Nom}} = V_N^2 \frac{P_{\text{rated}}}{S_{\text{rated}}^2}, L_{\text{Load}}^{\text{Nom}} = V_N^2 \frac{Q_{\text{rated}}}{S_{\text{rated}}^2} \frac{1}{\omega_N}, \quad (17)$$

where V_N and ω_N are the nominal voltage and frequency of the network respectively. By considering no-loading and overloading (200% loading) of GFM, it is assumed that $L_{\text{Load}} \in [\underline{L}_{\text{Load}}, \bar{L}_{\text{Load}}]$, $R_{\text{Load}} \in [\underline{R}_{\text{Load}}, \bar{R}_{\text{Load}}]$. As a result,

$$L_{\text{Load}} := L_{\text{Load}}^{\text{Nom}} + w_{\text{Load}}^L \delta_L, \quad (18)$$

$$R_{\text{Load}} := R_{\text{Load}}^{\text{Nom}} + w_{\text{Load}}^R \delta_R, \quad (19)$$

where, $\delta_L, \delta_R \in [-1, 1]$, $L_{\text{Load}}^{\text{Nom}} = \frac{1}{2}[\bar{L}_{\text{Load}} + \underline{L}_{\text{Load}}]$, $R_{\text{Load}}^{\text{Nom}} = \frac{1}{2}[\bar{R}_{\text{Load}} + \underline{R}_{\text{Load}}]$, $w_{\text{Load}}^L = \frac{1}{2}[\bar{L}_{\text{Load}} - \underline{L}_{\text{Load}}]$, and $w_{\text{Load}}^R = \frac{1}{2}[\bar{R}_{\text{Load}} - \underline{R}_{\text{Load}}]$.

3) *Generalized Representation of Uncertainty*: In synthesizing the controller with defined uncertainties in $R \in [\underline{R}, \bar{R}]$ and $L \in [\underline{L}, \bar{L}]$ when appearing in the form of $1/(Ls + R)$, linear fractional transformation (LFT) [46] can be utilized to convert the model into an upper LFT, $F_U(\mathbf{M}, \Delta)$, given as:

$$F_U(\mathbf{M}, \Delta) = \frac{1}{sL + R} = \mathbf{M}_{22} + \mathbf{M}_{21} \Delta [\mathbf{I} - \mathbf{M}_{11} \Delta]^{-1} \mathbf{M}_{12},$$

$$\text{with } \mathbf{M} = \begin{bmatrix} \mathbf{M}_{11} & \mathbf{M}_{12} \\ \mathbf{M}_{21} & \mathbf{M}_{22} \end{bmatrix}, \Delta = \begin{bmatrix} \delta_L & 0 \\ 0 & \delta_R \end{bmatrix}, \delta_L \in [-1, 1], \delta_R \in [-1, 1],$$

$$\mathbf{M}_{11} = \mathbf{M}_{22} \begin{bmatrix} s w^L & w^R \\ s w^L & w^R \end{bmatrix}, \mathbf{M}_{12} = \mathbf{M}_{22} \begin{bmatrix} 1 & 1 \\ 1 & 1 \end{bmatrix}^T, \mathbf{M}_{21} = \mathbf{M}_{22} \begin{bmatrix} s w^L & w^R \end{bmatrix},$$

where $\mathbf{M}_{22} = -1/[sL_{\text{Nom}} + R_{\text{Nom}}]$, $w^L = \frac{1}{2}[\bar{L} - \underline{L}]$, $w^R = \frac{1}{2}[\bar{R} - \underline{R}]$. It is important to note here that it is a generalized representation of uncertainty for both GFL and GFM inverter where $L = L_{\text{Th}}$, $R = R_{\text{Th}}$ for GFL inverter and $L = L_{\text{Load}}$, $R = R_{\text{Load}}$ for GFM inverter.

C. Shaping of Transfer Functions

The closed-loop objectives in designing the feedback control based on proposed robust controller, $\mathcal{C}_{H_\infty}(s)$, as shown in

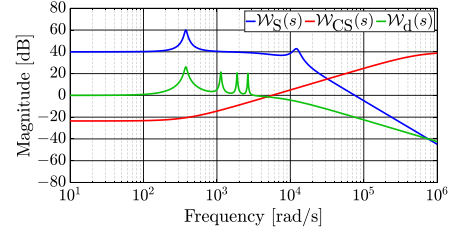


Fig. 6. Bode plots of magnitudes of selected weighting transfer functions.

Fig. 4 and Fig. 5 for GFL and GFM inverter, are as follows:
i) Reference Tracking : i_O tracks i_{ref} for GFL and v_O tracks v_{ref} for GFM inverter with minimum tracking error.
ii) Disturbance Rejection : Effects of v_{Th} on i_O for GFL and effect of i_h on v_O for GFM inverter are largely attenuated.
iii) Control Effort Reduction : v_{inv} satisfies the respective bandwidth limitations for GFL and GFM inverter.

Based on the objectives, user-defined weighting transfer functions, $\mathcal{W}_S(s)$, $\mathcal{W}_{CS}(s)$, $\mathcal{W}_d(s)$, are designed. The guidelines for designing the weighting functions are provided below.

1) *Selection of $\mathcal{W}_S(s)$* : To shape the sensitivity transfer function, the weighting function, $\mathcal{W}_S(s)$, is introduced so that **i)** The tracking error, e , ($e := i_{\text{ref}} - i_O$ and $e := v_{\text{ref}} - v_O$ for GFL and GFM inverter respectively) at fundamental frequency is small; **ii)** Resonance phenomenon of the system is actively damped.

$\mathcal{W}_S(s)$ is modeled to have peaks around ω_N and system's resonant frequency, ω_r (different in GFL and GFM open-loop plant), with 2nd order roll-off, $k_{S,1}(s)$ and formed as:

$$\mathcal{W}_S(s) = k_{S,1}(s) \frac{s^2 + 2k_{S,2}\zeta\omega_N s + \omega_N^2}{s^2 + 2\zeta\omega_N s + \omega_N^2} \frac{s^2 + 2k_{S,3}\zeta\omega_r s + \omega_r^2}{s^2 + 2\zeta\omega_r s + \omega_r^2},$$

where, $k_{S,2}$ and $k_{S,3}$ are selected to exhibit peaks and ζ addresses the off-nominal frequency around the nominal values.

2) *Selection of $\mathcal{W}_{CS}(s)$* : $\mathcal{W}_{CS}(s)$ is designed to suppress high-frequency control effort to shape the performance of v_{inv} for both GFL and GFM controller. Hence, it is designed as a high-pass filter with cut-off frequency at switching frequency for penalizing effect and is ascribed the form:

$$\mathcal{W}_{CS}(s) = k_{CS} \frac{s + k_{CS,1}\omega_N}{s + k_{CS,2}\omega_N}, \text{ where } k_{CS,1} \ll k_{CS,2}.$$

3) *Selection of $\mathcal{W}_d(s)$* : $\mathcal{W}_d(s)$ emphasizes the expected disturbances at fundamental and harmonic frequencies imposed by v_{Th} and i_h and emphasized by exogenous signal \hat{v}_{Th} and \hat{i}_h for GFL and GFM inverter respectively, as shown in Fig. 4 and Fig. 5. It is designed by a low-pass filter, $k_d(s)$, with peaks at selected frequencies and is ascribed the form:

$$\mathcal{W}_d(s) = k_d(s) \prod_{h=1,3,5,7} \frac{s^2 + 2k_{d,h}\zeta h\omega_N s + h^2\omega_N^2}{s^2 + 2\zeta h\omega_N s + h^2\omega_N^2},$$

where, the values of $k_{d,h}$ are selected based on the regulated limits of 3rd, 5th, 7th harmonics in network voltage and current injection with respect to fundamental [47]. A representative of selected weighting functions are shown in Fig. 6.

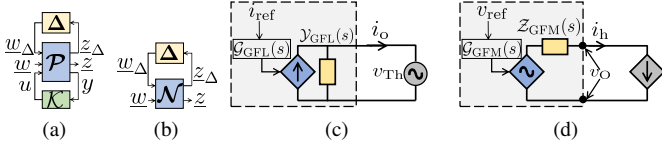


Fig. 7. Generalized (a) Δ - \mathcal{P} - \mathcal{K} control configuration, (b) Δ - \mathcal{N} control configuration, of Fig. 4 or Fig. 5 and closed-loop equivalent circuit model of (c) grid-following inverter system, (d) grid-forming inverter system.

D. Preparing the Generalized Plant

In preparation for robust controller design, $\mathcal{C}_{\mathcal{H}_\infty}(s)$, the multi-loop closed-loop block diagram in Fig. 4 and Fig. 5 for GFL and GFM inverter respectively are consolidated into the general control configuration in Fig. 7(a) [46]. Here, $\mathcal{P}(s)$ is the generalized multi-input-multi-output (MIMO) plant, $\mathcal{K}(s)$ is the proposed $\mathcal{C}_{\mathcal{H}_\infty}(s)$ controllers to be designed for GFL and GFM inverter and Δ is the structured uncertainty. w is a vector of the exogenous inputs (e.g., reference, disturbance), z are the exogenous outputs (e.g., signals to be regulated). y and u are the controller input and output signals respectively. z_Δ and w_Δ are the vector of input and output signals of structured uncertainty block. Note that in this continuous-time modeling framework, all variables are functions of the Laplace variable, s ; not explicitly shown for notational convenience. As a result, the generalized MIMO plant maps $[w_\Delta \ w \ u]^\top$ to $[z_\Delta \ z \ y]^\top$ as follows:

$$\begin{bmatrix} z_\Delta \\ z \\ y \end{bmatrix} = \begin{bmatrix} \mathcal{P}_{\Delta\Delta} & \mathcal{P}_{\Delta w} & \mathcal{P}_{\Delta u} \\ \mathcal{P}_{z\Delta} & \mathcal{P}_{zw} & \mathcal{P}_{zu} \\ \mathcal{P}_{y\Delta} & \mathcal{P}_{yw} & \mathcal{P}_{yu} \end{bmatrix} \begin{bmatrix} w_\Delta \\ w \\ u \end{bmatrix}, \quad (20)$$

where, the input and output signals are tabulated in Table I for both GFL and GFM inverter system. The detailed MIMO transfer function models of (20) for both GFL and GFM inverter systems are provided in Fig. 8 where

$$\begin{aligned} \mathcal{A}_{\text{GFL}} &= \frac{1}{[L_f C_f]s^2 + [R_f C_f]s + 1}, \\ \mathcal{B}_{\text{GFL}} &= \frac{L_f s + R_f}{[L_f C_f]s^2 + [R_f C_f]s + 1}, \\ \mathcal{A}_{\text{GFM}} &= \frac{1}{[L_f C_f]s^2 + [R_f C_f + L_f]s + [1 + R_f]}, \\ \mathcal{B}_{\text{GFM}} &= \frac{L_f s + R_f}{[L_f C_f]s^2 + [R_f C_f + L_f]s + [1 + R_f]}. \end{aligned}$$

If Δ is pulled out, then \mathcal{P} and \mathcal{K} can be clubbed together by a lower LFT to form \mathcal{N} in Fig. 7(b) as follows:

$$\begin{aligned} \mathcal{N} &= \begin{bmatrix} \mathcal{P}_{\Delta\Delta} & \mathcal{P}_{\Delta w} \\ \mathcal{P}_{z\Delta} & \mathcal{P}_{zw} \end{bmatrix} + \frac{\mathcal{K}}{[1 - \mathcal{P}_{yu}\mathcal{K}]^{-1}} \begin{bmatrix} \mathcal{P}_{\Delta u} \\ \mathcal{P}_{zu} \end{bmatrix} \begin{bmatrix} \mathcal{P}_{y\Delta} \\ \mathcal{P}_{yw} \end{bmatrix}^\top \\ &= \begin{bmatrix} \mathcal{N}_{\Delta\Delta} & \mathcal{N}_{\Delta w} \\ \mathcal{N}_{z\Delta} & \mathcal{N}_{zw} \end{bmatrix}, \text{ where } \begin{bmatrix} z_\Delta \\ z \end{bmatrix} = \mathcal{N} \begin{bmatrix} w_\Delta \\ w \end{bmatrix}. \end{aligned} \quad (21)$$

Therefore, the uncertainty closed-loop transfer function from w to z , $z = \mathcal{M}w$, is related to \mathcal{N} and Δ by an upper LFT where $\mathcal{M} = \mathcal{N}_{zw} + \mathcal{N}_{z\Delta}\Delta(\mathbf{I} - \mathcal{N}_{\Delta\Delta}\Delta)^{-1}\mathcal{N}_{\Delta w}$.

TABLE I
INPUT-OUTPUT MAPPING OF THE GENERALIZED PLANT

Signals	GFL Inverter	GFM Inverter
w	$[i_{\text{ref}} \ v_{\text{Th}}]^\top$ of Fig. 4	$[v_{\text{ref}} \ \dot{i}_h]^\top$ of Fig. 4
z	$[z_S \ z_{CS}]^\top$ of Fig. 4	$[z_S \ z_{CS}]^\top$ of Fig. 5
u	v_{inv} of Fig. 4	v_{inv} of Fig. 5
y	e of Fig. 4	e of Fig. 5
w_Δ	w_Δ of Fig. 4	w_Δ of Fig. 5
z_Δ	z_Δ of Fig. 4	z_Δ of Fig. 5

TABLE II
STABILITY ASSESSMENT OF RESULTING CONTROLLER

Controller	NS	NP	RS	RP
GFL Inverter	✓	0.49	0.91	0.94
GFM Inverter	✓	0.47	0.94	0.98

IV. CONTROLLER SYNTHESIS AND STABILITY ANALYSIS

With reference to the general control configuration of Fig. 7(a), the standard μ -synthesis-based optimal control problem is to find all stabilizing controllers $\mathcal{K}(s)$ by solving

$$\min_{\mathcal{K}(s) \text{ stabilizing}} \|\mathcal{N}\|_\infty, \quad (22)$$

where, $\|\cdot\|_\infty$ refers to the μ -synthesis norm. This problem can be readily solved using the MATLAB Robust Control Toolbox. An algorithm for solving (22) along with the theoretical underpinnings of this optimization problem can be found in [46]. Upon finding a stabilizing controller, the requirement of stability and performance of the closed-loop system are needed to be checked and can be summarized as follows:

Nominal Stable(NS) : \mathcal{N} is internally stable, (23)

Nominal Performance(NP) : $\|\mathcal{N}_{zw}\|_\infty < 1$ & NS, (24)

Robust Stable(RS) : $\mu_\Delta(\mathcal{N}_{\Delta\Delta}) < 1, \forall \omega$, & NS, (25)

Robust Performance(RP) : $\mu_{\bar{\Delta}}(\mathcal{N}) < 1, \forall \omega$, & NS, (26)

where, $\mu_\Delta(\mathcal{N}_{\Delta\Delta})$ and $\mu_{\bar{\Delta}}(\mathcal{N})$ are the structured singular values of $\mathcal{N}_{\Delta\Delta}$ and \mathcal{N} for the allowed structure of Δ and $\bar{\Delta} := \text{diag}(\Delta, \Delta_P)$ respectively with Δ_P being an unstructured uncertainty [46]. It is necessary to check whether stabilizing controller, $\mathcal{K}(s)$ of (22) satisfies all the conditions of (23)-(26) to analyze robust performance of the controller. In this work, an iterative approach is followed for μ -synthesis problem (i.e. finding the stabilizing controller that minimizes a given μ -condition). The parameters in either performance weights (i.e. $\mathcal{W}_S(s)$, $\mathcal{W}_{CS}(s)$, $\mathcal{W}_d(s)$) or uncertainty weights (i.e. w^L , w^R) are adjusted and then solved (22) until conditions of (23)-(26) are all satisfied. The optimal controller $\mathcal{K}(s)$ will have an order similar to the order of \mathcal{P} . Thus, before implementation in actual inverter control board, model order reduction is used to obtain a lower order controller using MATLAB's *balred* command. Moreover, bilinear transformation is used in the discretization stage of the resulting controller.

1) *Analysis of Resulting Controller for GFL Inverter:* Following the procedure of synthesizing the optimal controller for GFL inverter, a 13th order $\mathcal{C}_{\mathcal{H}_\infty}(s)$ of Fig. 4 is found to perform well. The closed-loop stability and desired performances are met as summarized in Table II. The closed-loop model for GFL inverter with negative feedback loop transfer function

Type	$\mathcal{P}(s)$ [$\mathcal{P}_{\Delta\Delta} \in \mathbb{C}^{2 \times 2}$, $\mathcal{P}_{\Delta w} \in \mathbb{C}^{2 \times 2}$, $\mathcal{P}_{\Delta u} \in \mathbb{C}^{2 \times 1}$, $\mathcal{P}_{z\Delta} \in \mathbb{C}^{2 \times 2}$, $\mathcal{P}_{zw} \in \mathbb{C}^{2 \times 2}$, $\mathcal{P}_{zu} \in \mathbb{C}^{2 \times 1}$, $\mathcal{P}_{y\Delta} \in \mathbb{C}^{1 \times 2}$, $\mathcal{P}_{yw} \in \mathbb{C}^{1 \times 2}$, $\mathcal{P}_{yu} \in \mathbb{C}$]		
GFL	$\mathcal{P}_{\Delta\Delta} = \mathbf{M}_{11} - \frac{\mathcal{B}_{GFL}}{1 + M_{22}\mathcal{B}_{GFL}} \mathbf{M}_{12}\mathbf{M}_{21}$	$\mathcal{P}_{\Delta w} = \begin{bmatrix} \mathbf{0}_{2 \times 1} & \mathcal{B}_{GFL} W_d M_{22} \\ & 1 + M_{22}\mathcal{B}_{GFL} \end{bmatrix} \mathbf{M}_{12}$	$\mathcal{P}_{\Delta u} = \left(\mathcal{A}_{GFL} - \frac{\mathcal{B}_{GFL} \mathcal{A}_{GFL} M_{22}}{1 + M_{22}\mathcal{B}_{GFL}} \mathbf{M}_{12} \right) \mathbf{M}_{12}$
	$\mathcal{P}_{z\Delta} = \begin{bmatrix} -\frac{W_S}{1 + M_{22}\mathcal{B}_{GFL}} \mathbf{M}_{21} \\ \mathbf{0}_{1 \times 2} \end{bmatrix}$	$\mathcal{P}_{zw} = \begin{bmatrix} W_S & \mathcal{B}_{GFL} W_d M_{22} \\ 0 & 1 + M_{22}\mathcal{B}_{GFL} \end{bmatrix}$	$\mathcal{P}_{zu} = \begin{bmatrix} -\frac{W_S M_{22} \mathcal{A}_{GFL}}{1 + M_{22}\mathcal{B}_{GFL}} \\ W_{CS} \end{bmatrix}$
	$\mathcal{P}_{y\Delta} = -\frac{1}{1 + M_{22}\mathcal{B}_{GFL}} \mathbf{M}_{21}$	$\mathcal{P}_{yw} = 1 - \frac{M_{22} W_d}{1 + M_{22}\mathcal{B}_{GFL}}$	$\mathcal{P}_{yu} = -\frac{M_2 \mathcal{A}_{GFL}}{1 + M_{22}\mathcal{B}_{GFL}}$
GFM	$\mathcal{P}_{\Delta\Delta} = \mathbf{M}_{11} - \mathcal{B}_{GFM} \mathbf{M}_{12} \mathbf{M}_{21}$	$\mathcal{P}_{\Delta w} = \begin{bmatrix} \mathbf{0}_{2 \times 1} & -W_d \mathcal{B}_{GFM} \mathbf{M}_{12} \\ & 1 \end{bmatrix}$	$\mathcal{P}_{\Delta u} = \mathcal{A}_{GFM} \mathbf{M}_{12}$
	$\mathcal{P}_{z\Delta} = \begin{bmatrix} -W_S \mathcal{B}_{GFM} \mathbf{M}_{21} \\ \mathbf{0}_{1 \times 2} \end{bmatrix}$	$\mathcal{P}_{zw} = \begin{bmatrix} W_S & -W_S W_d \mathcal{B}_{GFM} \\ 0 & 1 \end{bmatrix}$	$\mathcal{P}_{zu} = \begin{bmatrix} -W_S \mathcal{A}_{GFM} \\ W_{CS} \end{bmatrix}$
	$\mathcal{P}_{y\Delta} = \mathcal{B}_{GFM} \mathbf{M}_{21}$	$\mathcal{P}_{yw} = 1 - W_d \mathcal{B}_{GFM}$	$\mathcal{P}_{yu} = -\mathcal{A}_{GFM}$

Fig. 8. The generalized MIMO transfer function models, $\mathcal{P}(s)$, of (20) for both GFL inverter control of Fig. 4 and GFM inverter control of Fig. 5.

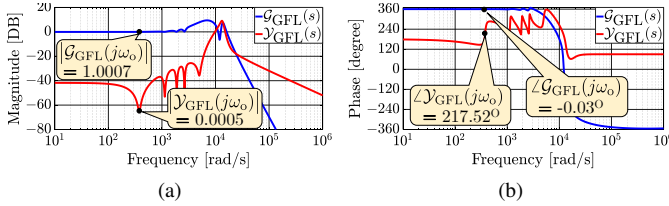


Fig. 9. Bode plots, (a) magnitudes, (b) phase, of \mathcal{G}_{GFL} , \mathcal{Y}_{GFL} of Fig. 7(c).

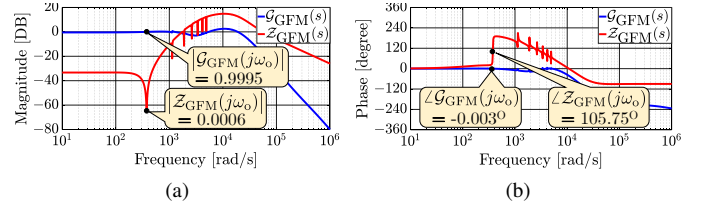


Fig. 10. Bode plots, (a) magnitudes, (b) phase, of \mathcal{G}_{GFM} , \mathcal{Z}_{GFM} of Fig. 7(d).

with resulting controller, $\mathcal{C}_{\mathcal{H}\infty}(s)$, in Fig. 4 can be derived by substituting $v_{inv}(s) = \mathcal{C}_{\mathcal{H}\infty}(s)[i_{ref} - i_O]$ in (4). It can be written as $i_O = \mathcal{G}_{GFL}(s)i_{ref} - \mathcal{Y}_{GFL}(s)v_{Th}$ and represented as Norton's equivalent model connected to a voltage source as shown in Fig. 7(c). For an example, at nominal plant condition with resulting optimal controller, the Bode plot of $\mathcal{G}_{GFL}(s)$ and $\mathcal{Y}_{GFL}(s)$ are shown in Fig. 9(a) and Fig. 9(b) respectively. It is observed that $|\mathcal{G}_{GFL}(j\omega_N)|$, $\angle \mathcal{G}_{GFL}(j\omega_N)$ and $|\mathcal{Y}_{GFL}(j\omega_N)|$ are ≈ 1 , $\approx 0^\circ$ and ≈ 0 respectively that leads to $i_O \approx i_{ref}$ at fundamental frequency.

2) *Analysis of Resulting Controller for GFM Inverter:* Following the procedure of synthesizing the optimal controller for GFM inverter, a 14th order $\mathcal{C}_{\mathcal{H}\infty}(s)$ of Fig. 5 is found to be sufficient and performs well. The closed-loop stability and desired performances are met as summarized in Table II. The closed-loop model for GFM inverter with negative feedback loop transfer function with resulting controller, $\mathcal{C}_{\mathcal{H}\infty}(s)$, in Fig. 5 can be derived by substituting $v_{inv}(s) = \mathcal{C}_{\mathcal{H}\infty}(s)[v_{ref} - v_O]$ in (13). It can be written as $v_O = \mathcal{G}_{GFM}(s)v_{ref} - \mathcal{Z}_{GFM}(s)i_h$ and represented as Thevenin's equivalent model connected across a current source as shown in Fig. 7(d). For an example, at nominal plant condition with resulting optimal controller, the Bode plot of $\mathcal{G}_{GFM}(s)$ and $\mathcal{Z}_{GFM}(s)$ are shown in Fig. 10(a) and Fig. 10(b) respectively. It is observed that $|\mathcal{G}_{GFM}(j\omega_N)|$, $\angle \mathcal{G}_{GFM}(j\omega_N)$ and $|\mathcal{Z}_{GFM}(j\omega_N)|$ are ≈ 1 , $\approx 0^\circ$ and ≈ 0 respectively that leads to $v_O \approx v_{ref}$ at fundamental frequency.

V. EXPERIMENTAL RESULTS AND VERIFICATION

A. Experimental Configuration

A combined system-in-the-loop (SIL), controller hardware-in-the-loop (CHIL) and power hardware-in-the-loop (PHIL) based experimental validation is conducted in order to evaluate the efficacy and viability of the proposed μ -synthesis-based controller for single-phase GFL and GFM inverters. The

TABLE III
1-PHASE INVERTER SYSTEM UNDER STUDY

Inverter	Value
Ratings (1- ϕ)	240 V, 60 Hz, 1.67 kVA, 0.9 pf
Inverter Parameters	$V_{dc} = 500$ V, $f_{sw} = 20$ kHz
Filter Parameters	$L_f = 2$ mH, $R_f = 0.2$ Ω , $C_f = 20$ μ F

ratings and parameters of the inverter systems are tabulated in Table III. The laboratory-based experimental setup is shown in Fig. 11(a). The configuration is shown in Fig. 11(b) and described below:

1) *Real-time Simulation and SIL Configuration:* A residential sub-network of North American low voltage distribution feeder from CIGRE Task Force C6.04.02 [48], affiliated with CIGRE Study Committee C6 is emulated using eMEGASIM platform inside the OP5700 RT-simulator (RTS) manufactured by OPAL-RT. The original ratings of load at each bus and line parameters are modified in order to make it compatible with the voltage rating and power capacity of the laboratory. Moreover, the test system is modified by including sufficient non-linear loads at various buses while respecting the recommended limits of harmonic distortions mentioned in [47]. As part of SIL-setup, one GFM and one GFL inverter are emulated entirely (i.e. both power circuit and the control with proposed μ -synthesis-based controller) inside the RTS, connected at Bus₁ and Bus₁₂ respectively as shown in Fig. 11(b).

2) *Controller Hardware-in-the-loop Configuration:* As part of CHIL-setup, one GFM and one GFL inverter system are emulated with only power circuit inside the RTS, connected at Bus₁₀ and Bus₁₄ respectively as shown in Fig. 11(b). The proposed μ -synthesis-based control logic of both GFL and GFM inverter systems are realized on two Texas-Instruments TMS320F28379D, 16/12-bit floating-point 200 MHz Delfino micro-controller boards interfaced with RTS.

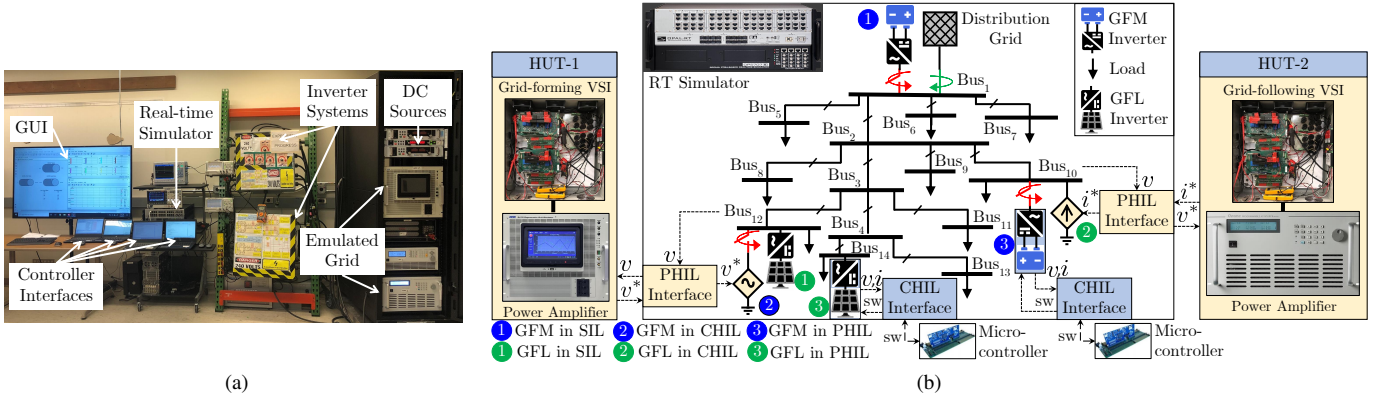


Fig. 11. (a) The laboratory-based experimental hardware setup, (b) the configuration of SIL-CHIL-PHIL-based experimental setup.

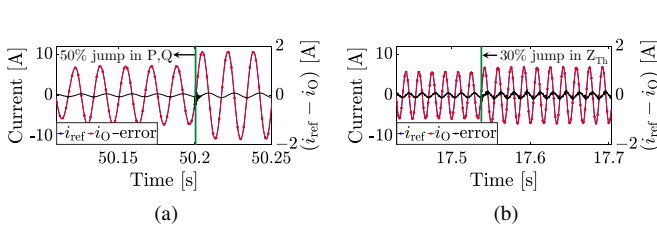


Fig. 12. The current reference tracking capability of GFL inverter with proposed μ -synthesis-based optimal controller in CHIL setup at Bus₁₄ of Fig. 11(b) in (a) CASE-1, (b) CASE-2.

3) *Power Hardware-in-the-loop Configuration*: As part of PHIL-setup, one GFM (HUT-1 in Fig. 11(b)) and one GFL inverter (HUT-2 in Fig. 11(b)), connected at Bus₁₂ and Bus₁₀ respectively, are physically realized outside the RTS. The ideal transformer model (ITM) based PHIL interface logic [49] is adapted for both the hardware-under-tests (HUTs'). In HUT-1 the physical inverter system, fed by MAGNA-POWER programmable DC power supply, is interfaced with low-cost Texas-Instruments TMS320F28379D, 16/12-bit floating-point 200 MHz Delfino micro-controller boards employed with proposed μ -synthesis control logic for GFM inverter. The power terminals of the inverter are connected with a power amplifier realized by NHR 9410 regenerative grid simulator. On the other hand, in HUT-2 the physical inverter system, fed by another MAGNA-POWER programmable DC power supply, is interfaced with another low-cost Texas-Instruments TMS320F28379D, 16/12-bit floating-point 200 MHz Delfino micro-controller boards employed with proposed μ -synthesis control logic for GFL inverter. The power terminals of the inverter are connected with a power amplifier realized by Chroma 61605 programmable ac power source.

B. Results and Discussions

Four test cases (two test cases each for GFL and GFM inverters) are demonstrated by emulating a sequence of events. Two test cases for GFL inverters are as follows:

- CASE-1: The emulated distribution network of Fig. 11(b) is running in off-grid mode and P-Q reference of GFL inverters jumps up by 50% due to increased demand.
- CASE-2: The network is running in off-grid mode and experiences a topology change which results in 30% increase

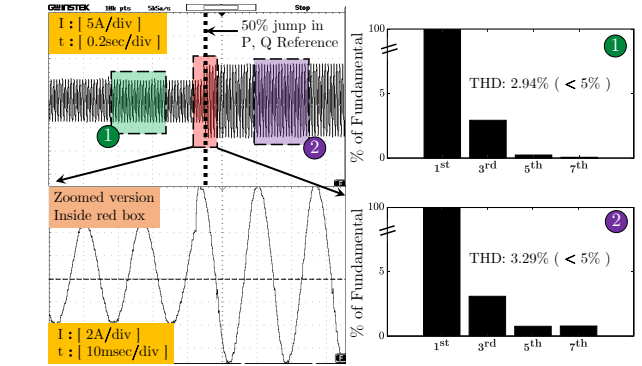


Fig. 13. The current reference tracking capability of GFL inverter in PHIL setup at Bus₁₀ of Fig. 11(b) in CASE-1 with the proposed optimal controller.

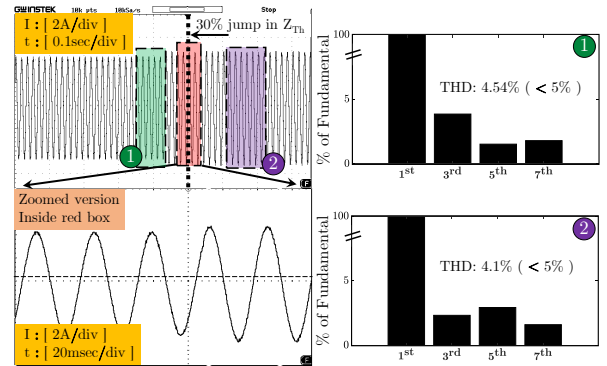


Fig. 14. The current reference tracking capability of GFL inverter in PHIL setup at Bus₁₀ of Fig. 11(b) in CASE-2 with the proposed optimal controller.

in equivalent Thevenin impedance at PCC of GFM inverters.

- CASE-3: The emulated distribution network of Fig. 11(b) has an on-grid to off-grid mode transition. GFM inverters will have a maximum jump in loading from no-load condition (during on-grid mode) to full-load condition (during off-grid mode).
- CASE-4: The same network has an off-grid to on-grid mode transition. GFM inverters will have another maximum jump in loading from full-load condition (during off-grid mode) to no-load condition (during on-grid mode). Clearly, CASE-1, CASE-2 and CASE-3, CASE-4 are designed in order to capture the robust performance of proposed GFL and GFM control during maximal model uncertainty respectively.

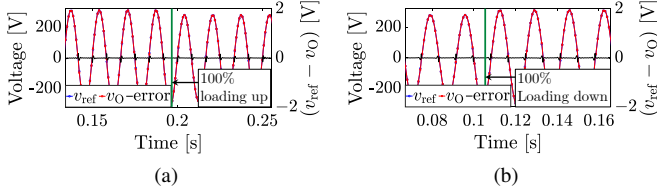


Fig. 15. The voltage reference tracking capability of GFM inverter with the proposed μ -synthesis-based optimal controller in CHIL setup at Bus₁₀ of Fig. 11(b) in (a) CASE-3 and (b) CASE-4.

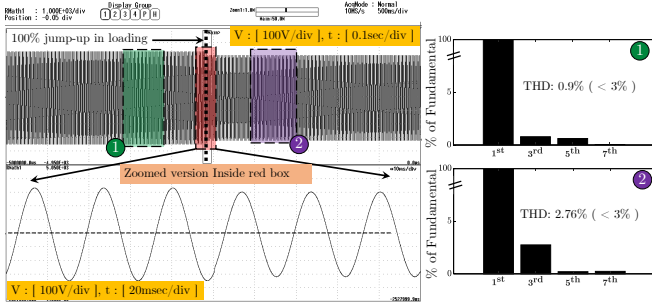


Fig. 16. The voltage reference tracking capability of GFM inverter in PHIL setup at Bus₁₂ of Fig. 11(b) in CASE-3 with the proposed optimal controller.

Fig. 12(a) and Fig. 12(b) show the current reference tracking capability of the proposed μ -synthesis-based optimal controller for GFL inverter (at Bus₁₄ of Fig. 11(b)) in CHIL demonstration of CASE-1 and CASE-2 respectively. RMS instantaneous current tracking error (rICTE in %), defined as $100 \times \text{RMS}(i_{\text{ref}} - i_O) / [\sqrt{2} \text{RMS}(i_{\text{ref}})]$, is used for assessing the tracking performance of the current controller. It is observed in Fig. 12(a) that both the current reference and output current increases during 50% increase in P-Q set-points due to adopted reference generation of Appendix A. The proposed optimal controller has significantly small error in current reference tracking before (rICTE \approx 1.7%) and after (rICTE \approx 1.9%) the transition in CASE-1. Similarly, Fig. 12(b) shows that the proposed optimal controller has significantly small error in current reference tracking before (rICTE \approx 1.9%) and after (rICTE \approx 2.1%) the jump of equivalent Thevenin impedance in CASE-2. Fig. 13 shows the current response of GFL inverter (HUT-2 at Bus₁₀ of Fig. 11(b)) as a part of PHIL demonstration of the same event. Here the result is focused on determining the harmonic compensation capability of the proposed optimal controller for GFL inverter during varying reference set-point. It is observed that the total demand distortion (TDD) of current waveform is $< 5\%$ before and after the transition as recommended in [47]. Thus, the proposed μ -synthesis-based controller for GFL inverter shows good reference tracking and harmonic compensation capability in CASE-1. Similarly, Fig. 14 shows the current response of GFL inverter (HUT-2 at Bus₁₀ of Fig. 11(b)) as a part of PHIL demonstration of the same event. Here the result is focused on determining the harmonic compensation capability of the proposed μ -synthesis-based optimal controller for GFL inverter during model uncertainty. It is observed here that the TDD of current waveform is $< 5\%$ before and after the transition as recommended in [47]. Thus,

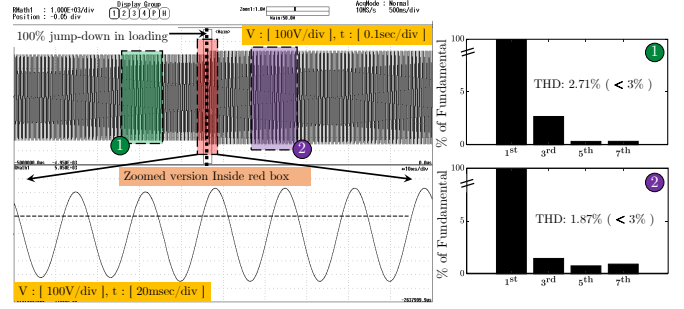


Fig. 17. The voltage reference tracking capability of GFM inverter in PHIL setup at Bus₁₂ of Fig. 11(b) in CASE-4 with the proposed optimal controller.

the data corroborates the efficacy of the proposed μ -synthesis-based controller for GFL inverter for good reference tracking and harmonic compensation capability in CASE-2. The CHIL and PHIL results substantiate the fact that the proposed μ -synthesis-based optimal controller for GFL is showing robust performance by making sure to have good reference tracking, disturbance rejection and harmonic compensation capability under significant in the plant model uncertainty.

Fig. 15(a) and Fig. 15(b) show the voltage reference tracking capability of the proposed μ -synthesis-based optimal controller for GFM inverter (at Bus₁₀ of Fig. 11(b)) in CHIL demonstration of CASE-3 and CASE-4 respectively. RMS instantaneous voltage tracking error (rIVTE in %), defined as $100 \times \text{RMS}(v_{\text{ref}} - v_O) / [\sqrt{2} \text{RMS}(v_{\text{ref}})]$, is used for assessing the tracking performance of the voltage controller. It is observed in Fig. 15(a) that both the voltage reference and output voltage drop during jump in loading (no-load to full-load) due to adopted droop-controlled reference generation of Appendix B. The proposed μ -synthesis-based optimal controller has significantly small error in voltage reference tracking as shown in Fig. 15(a) before (rIVTE \approx 0.2%) and after (rIVTE \approx 0.1%) the increase of equivalent loading. Similarly, it is observed in Fig. 15(b) that both the voltage reference and output voltage, increase during drop in loading (full-load to no-load). The proposed optimal controller has significantly small error in voltage reference tracking before (rIVTE \approx 0.2%) and after (rIVTE \approx 0.1%) the decrease in equivalent loading. Fig. 16 shows the voltage response of GFM inverter (HUT-1 at Bus₁₂ of Fig. 11(b)) as a part of PHIL demonstration of the same event. Here the result is focused on determining the harmonic compensation capability of the proposed optimal controller for GFM inverter during model uncertainty change due to loading. It is observed that the total harmonic distortion (THD) of voltage waveform is $< 3\%$ before and after the transition. This is significantly less than the voltage distortion limit ($< 8\%$) as recommended in [47]. Thus the data corroborates the advantage of the proposed μ -synthesis-based controller for GFM inverter shows robust performance during model uncertainty caused in CASE-3. Similarly, Fig. 17 shows the voltage response of GFM inverter (HUT-1 at Bus₁₂ of Fig. 11(b)) as a part of PHIL demonstration of the same event. Here the result is focused on determining the harmonic compensation capability of the proposed optimal controller for GFM inverter during model uncertainty change due to loading. It is observed that

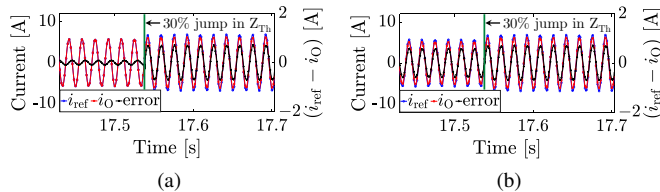


Fig. 18. The current reference tracking capability of GFL inverter in CHIL setup at Bus₁₄ of Fig. 11(b) with, (a) \mathcal{H}_∞ -based controller without considering uncertainty of Thevenin impedance, (b) the classical PR controller.

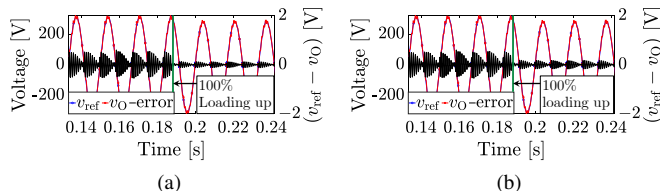


Fig. 19. The voltage reference tracking capability of GFM inverter in CHIL setup at Bus₁₀ of Fig. 11(b) with, (a) \mathcal{H}_∞ -based controller without considering uncertainty of equivalent loading, (b) the classical PR controller.

total harmonic distortion (THD) of voltage waveform is $< 3\%$ before and after the transition. This is significantly less than the voltage distortion limit ($< 8\%$) as recommended in [47]. Thus GFM inverter shows robust performance during model uncertainty caused in CASE-4. The CHIL and PHIL results substantiate the fact that the proposed optimal controller for GFM is showing robust performance by having good reference tracking, disturbance rejection and harmonic compensation capability under significant in the plant model uncertainty.

C. Performance Comparison

To showcase the robust performance of the proposed μ -synthesis-based controller, a nominal \mathcal{H}_∞ -based robust controller and a classical PR-based controllers are designed for comparison purpose. For GFL inverter, the \mathcal{H}_∞ -based robust controller is designed by considering the nominal value of Thevenin impedance. Whereas, for GFM inverter, the \mathcal{H}_∞ -based robust controller is designed considering 100% equivalent loading as nominal. Fig. 18(a) and Fig. 18(b) show the current reference tracking capability of the \mathcal{H}_∞ -based and PR-based current controller for GFL inverter (at Bus₁₄ of Fig. 11(b)) in CHIL demonstration of CASE-2 respectively. It is observed that the nominal \mathcal{H}_∞ -based robust controller has significant error in current reference tracking (rICTE increases from $\approx 2.5\%$ to $\approx 10\%$) after 30% jump in equivalent Thevenin impedance from nominal value. Whereas, the PR-based controller has comparatively larger error both before (rICTE $\approx 6\%$) and after (rICTE $\approx 10\%$) the transition of CASE-2. Whereas, the proposed μ -synthesis-based optimal controller has significantly small error in current reference tracking before (rICTE $\approx 1.9\%$) and after (rICTE $\approx 2.1\%$) the jump of equivalent Thevenin impedance in CASE-2 as shown in Fig. 12(b). Similarly, Fig. 19(a) and Fig. 19(b) show the voltage reference tracking capability of the \mathcal{H}_∞ -based and PR-based voltage controller for GFM inverter (at Bus₁₀ of Fig. 11(b)) in CHIL demonstration of CASE-3 respectively. It is observed that the nominal \mathcal{H}_∞ -based robust

controller has significant error in voltage reference tracking (rIVTE $\approx 1.2\%$) at no-load condition. Whereas, the PR-based controller has comparatively larger error both before (rIVTE $\approx 1.4\%$) and after (rIVTE $\approx 0.8\%$) the transition of CASE-3. Whereas, the proposed μ -synthesis-based optimal controller has significantly small error in voltage reference tracking before (rIVTE $\approx 0.2\%$) and after (rIVTE $\approx 0.1\%$) the increase of equivalent loading as shown in Fig. 15(a).

VI. CONCLUSION

In this article, a generalized μ -synthesis-based robust control framework is proposed utilizing the fact that there is a voltage-current duality in the plant dynamic model of GFL and GFM inverter. The uncertainties in grid impedance parameters and uncertainties in equivalent loading parameters for GFL and GFM inverters are modeled respectively. The generalized control framework results the controllers that are single-loop, hence simple and cost-effective enough to be implemented, and optimal, in the sense of robustness in performance under uncertainties. The resulting current-controller for GFL inverter provides inherent active damping under grid parameter variation whereas the resulting voltage-controller for GFM inverter enhances the dynamic performance during load transients. A SIL-CHIL-PHIL-based experimental validation evaluates the efficacy and viability of the proposed controllers.

APPENDIX

Appendix A: Reference Generation for Grid-following Inverter

The outer ‘Reference Generation Block’ of Fig. 2(a) eventually generates the i_{ref} signal using its pre-specified reference active power, P_{ref} , and reactive power, Q_{ref} , (defined locally/centrally) and output signals from phase-locked loop (PLL). The expression of i_{ref} is given by

$$i_{\text{ref}} = \sqrt{2} \frac{\sqrt{P_{\text{ref}}^2 + Q_{\text{ref}}^2}}{\tilde{V}} \sin \left(\tilde{\theta} - \arctan \frac{Q_{\text{ref}}}{P_{\text{ref}}} \right), \quad (27)$$

where, a $1-\phi$ second order generalized integrator-based synchronous reference frame PLL (SOGI-SRF-PLL) operates with its grid-synchronization technique and generates the RMS value, \tilde{V} , and synchronized phase information, $\tilde{\theta}$, of v_o [50].

Appendix B: Reference Generation for Grid-forming Inverter

A P - f/Q - V droop control strategy is adopted for outer ‘Reference Generation Block’ of Fig. 2(b). The droop characteristic equations are as follows [51]:

$$\omega = \omega_N - n_P P, \quad V = V_N - m_Q Q, \quad (28)$$

$$v_{\text{ref}} = \sqrt{2} V \sin \left(\int \omega dt \right), \quad (29)$$

where, ω_N and V_N are nominal frequency (in rad/sec) and voltage (RMS) respectively. P and Q are averaged active and reactive power output of GFM inverter. n_P and m_Q are the droop coefficients and the values are typically chosen such that ω and V are within the allowed specification, defined by IEEE 1547 Standard [45], for all $P \in [0, P_{\text{rated}}]$ and $Q \in [-Q_{\text{rated}}, Q_{\text{rated}}]$ respectively. Here, P_{rated} and Q_{rated} are the rated active and reactive power of the GFM inverter.

REFERENCES

- [1] J. P. Lopes, C. Moreira, and A. Madureira, "Defining control strategies for microgrids islanded operation," *IEEE Transactions on power systems*, vol. 21, no. 2, pp. 916–924, 2006.
- [2] A. Bidram and A. Davoudi, "Hierarchical structure of microgrids control system," *IEEE Transactions on Smart Grid*, vol. 3, no. 4, 2012.
- [3] J. Xu, S. Xie, B. Zhang, and Q. Qian, "Robust grid current control with impedance-phase shaping for lcl-filtered inverters in weak and distorted grid," *IEEE Transactions on Power Electronics*, vol. 33, no. 12, pp. 10 240–10 250, 2018.
- [4] C. Kammer, S. D'Arco, A. G. Endegnanew, and A. Karimi, "Convex optimization-based control design for parallel grid-connected inverters," *IEEE Transactions on Power Electronics*, vol. 34, no. 7, 2018.
- [5] L. Zhou, X. Zhou, Y. Chen, Z. Lv, Z. He, W. Wu, L. Yang, K. Yan, A. Luo, and J. M. Guerrero, "Inverter-current-feedback resonance-suppression method for lcl-type dg system to reduce resonance-frequency offset and grid-inductance effect," *IEEE Transactions on Industrial Electronics*, vol. 65, no. 9, pp. 7036–7048, 2018.
- [6] W. Zhou, N. Mohammed, and B. Bahrani, "Comprehensive modeling, analysis, and comparisons of state-space and impedance models of pll-based grid-following inverters considering different outer control modes," *IEEE Access*, 2022.
- [7] C. Xie, X. Zhao, K. Li, J. Zou, and J. M. Guerrero, "A new tuning method of multiresonant current controllers for grid-connected voltage source converters," *IEEE Journal of Emerging and Selected Topics in Power Electronics*, vol. 7, no. 1, pp. 458–466, 2018.
- [8] L. Harnefors, J. Kukkola, M. Routimo, M. Hinkkanen, and X. Wang, "A universal controller for grid-connected voltage-source converters," *IEEE Journal of Emerging and Selected Topics in Power Electronics*, vol. 9, no. 5, pp. 5761–5770, 2020.
- [9] J. Jiao, J. Y. Hung, and R. Nelms, "State feedback control for single-phase grid-connected inverter under weak grid," in *2017 IEEE 26th International Symposium on Industrial Electronics (ISIE)*. IEEE, 2017, pp. 879–885.
- [10] M. G. Taul, C. Wu, S.-F. Chou, and F. Blaabjerg, "Optimal controller design for transient stability enhancement of grid-following converters under weak-grid conditions," *IEEE Transactions on Power Electronics*, vol. 36, no. 9, pp. 10 251–10 264, 2021.
- [11] K. Arulkumar, P. Manojbharath, S. Meikandasivam, and D. Vijayakumar, "Robust control design of grid power converters in improving power quality," in *2015 International Conference on Technological Advancements in Power and Energy (TAP Energy)*. IEEE, 2015, pp. 460–465.
- [12] M. Ebrahimi, S. A. Khajehoddin, and M. Karimi-Ghartemani, "Fast and robust single-phase dq current controller for smart inverter applications," *IEEE transactions on power electronics*, vol. 31, no. 5, 2015.
- [13] E. Twining and D. G. Holmes, "Grid current regulation of a three-phase voltage source inverter with an lcl input filter," *IEEE transactions on power electronics*, vol. 18, no. 3, pp. 888–895, 2003.
- [14] W. Wu, Y. He, and F. Blaabjerg, "An lcl power filter for single-phase grid-tied inverter," *IEEE Transactions on Power Electronics*, vol. 27, no. 2, pp. 782–789, 2011.
- [15] I. J. Gabe, V. F. Montagner, and H. Pinheiro, "Design and implementation of a robust current controller for vsi connected to the grid through an lcl filter," *IEEE Transactions on Power Electronics*, vol. 24, no. 6, pp. 1444–1452, 2009.
- [16] A. Timbus, M. Liserre, R. Teodorescu, P. Rodriguez, and F. Blaabjerg, "Evaluation of current controllers for distributed power generation systems," *IEEE Transactions on power electronics*, vol. 24, no. 3, pp. 654–664, 2009.
- [17] J. N. da Silva, A. J. Sguarez Filho, D. A. Fernandes, A. P. Tahim, E. R. da Silva, and F. F. Costa, "A discrete repetitive current controller for single-phase grid-connected inverters," in *2017 Brazilian Power Electronics Conference (COBEP)*. IEEE, 2017, pp. 1–6.
- [18] H. M. Kojabadi, B. Yu, I. A. Gadoura, L. Chang, and M. Ghribi, "A novel dsp-based current-controlled pwm strategy for single phase grid connected inverters," *IEEE transactions on power electronics*, vol. 21, no. 4, pp. 985–993, 2006.
- [19] M. Huang, Q. Tan, H. Li, and W. Wu, "Improved sliding mode control method of single-phase lcl filtered vsi," in *2018 9th IEEE International Symposium on Power Electronics for Distributed Generation Systems (PEDG)*. IEEE, 2018, pp. 1–5.
- [20] Leming Zhou, An Luo, Y. Chen, Xiaoping Zhou, and Zhiyong Chen, "A novel two degrees of freedom grid current regulation for single-phase lcl-type photovoltaic grid-connected inverter," in *2016 IEEE 8th International Power Electronics and Motion Control Conference (IPEMC-ECCE Asia)*, May 2016, pp. 1596–1600.
- [21] T. Hornik and Q.-C. Zhong, "A current-control strategy for voltage-source inverters in microgrids based on h ∞ and repetitive control," *IEEE Transactions on Power Electronics*, vol. 26, no. 3, pp. 943–952, 2010.
- [22] S. Chakraborty, S. Patel, and M. V. Salapaka, "Design of H ∞ -based robust controller for single-phase grid-feeding voltage source inverters," in *2020 52nd North American Power Symposium*. IEEE, 2021, pp. 1–6.
- [23] J. Wang, I. Tyurukanov, and A. Monti, "Design of a novel robust current controller for grid-connected inverter against grid impedance variations," *International Journal of Electrical Power & Energy Systems*, vol. 110, pp. 454–466, 2019.
- [24] S. Yang, Q. Lei, F. Z. Peng, and Z. Qian, "A robust control scheme for grid-connected voltage-source inverters," *IEEE Transactions on Industrial Electronics*, vol. 58, no. 1, pp. 202–212, 2010.
- [25] A. Yazdani and R. Iravani, *Voltage-sourced converters in power systems*. Wiley Online Library, 2010, vol. 34.
- [26] Y. Wu and Y. Ye, "Internal model-based disturbance observer with application to cvcf pwm inverter," *IEEE Transactions on Industrial Electronics*, vol. 65, no. 7, pp. 5743–5753, 2018.
- [27] P. Unruh, M. Nuschke, P. Strauß, and F. Welck, "Overview on grid-forming inverter control methods," *Energies*, vol. 13, no. 10, 2020.
- [28] P. C. Loh, M. J. Newman, D. N. Zmood, and D. G. Holmes, "A comparative analysis of multiloop voltage regulation strategies for single and three-phase ups systems," *IEEE Transactions on Power Electronics*, vol. 18, no. 5, pp. 1176–1185, 2003.
- [29] Y. Li, Y. Gu, Y. Zhu, A. Junyent-Ferré, X. Xiang, and T. C. Green, "Impedance circuit model of grid-forming inverter: Visualizing control algorithms as circuit elements," *IEEE Transactions on Power Electronics*, vol. 36, no. 3, pp. 3377–3395, 2020.
- [30] X. Quan, "Improved dynamic response design for proportional resonant control applied to three-phase grid-forming inverter," *IEEE Transactions on Industrial Electronics*, vol. 68, no. 10, pp. 9919–9930, 2020.
- [31] H. Wu, D. Lin, D. Zhang, K. Yao, and J. Zhang, "A current-mode control technique with instantaneous inductor-current feedback for ups inverters," in *APEC'99. Fourteenth Annual Applied Power Electronics Conference and Exposition. 1999 Conference Proceedings (Cat. No. 99CH36285)*, vol. 2. IEEE, 1999, pp. 951–957.
- [32] Q. Lei, F. Z. Peng, and S. Yang, "Multiloop control method for high-performance microgrid inverter through load voltage and current decoupling with only output voltage feedback," *IEEE Transactions on Power Electronics*, vol. 26, no. 3, pp. 953–960, 2010.
- [33] D. Dong, T. Thacker, R. Burgos, F. Wang, and D. Boroyevich, "On zero steady-state error voltage control of single-phase pwm inverters with different load types," *IEEE Transactions on Power Electronics*, vol. 26, no. 11, pp. 3285–3297, 2011.
- [34] Tzann-Shin Lee, S. . Chiang, and Jhy-Ming Chang, "H ∞ loop-shaping controller designs for the single-phase ups inverters," *IEEE Transactions on Power Electronics*, vol. 16, no. 4, pp. 473–481, July 2001.
- [35] J. Teng, W. Gao, D. Czarkowski, and Z.-p. Jiang, "Optimal tracking with disturbance rejection of voltage source inverters," *IEEE Transactions on Industrial Electronics*, 2019.
- [36] G. Weiss, Q.-C. Zhong, T. C. Green, and J. Liang, "H ∞ repetitive control of dc-ac converters in microgrids," *IEEE Transactions on Power Electronics*, vol. 19, no. 1, pp. 219–230, 2004.
- [37] G. Willmann, D. F. Coutinho, L. F. A. Pereira, and F. B. Líbano, "Multiple-loop h-infinity control design for uninterruptible power supplies," *IEEE Transactions on Industrial Electronics*, vol. 54, no. 3, pp. 1591–1602, 2007.
- [38] B. B. Johnson, B. R. Lundstrom, S. Salapaka, and M. Salapaka, "Optimal structures for voltage controllers in inverters," National Renewable Energy Lab.(NREL), Golden, CO (United States), Tech. Rep., 2018.
- [39] M. Hamzeh, S. Emamian, H. Karimi, and J. Mahseredjian, "Robust control of an islanded microgrid under unbalanced and nonlinear load conditions," *IEEE Journal of Emerging and Selected Topics in Power Electronics*, vol. 4, no. 2, pp. 512–520, 2015.
- [40] M. A. U. Rasool, M. M. Khan, Z. Ahmed, and M. A. Saeed, "Analysis of an h ∞ robust control for a three-phase voltage source inverter," *Inventions*, vol. 4, no. 1, p. 18, 2019.
- [41] S. Chakraborty, S. Patel, and M. V. Salapaka, "Robust and optimal single-loop voltage controller for grid-forming voltage source inverters," in *2020 IEEE Power and Energy Conference at Illinois (PECI)*. IEEE, 2020, pp. 1–7.
- [42] Z. Li, C. Zang, P. Zeng, H. Yu, S. Li, and J. Bian, "Control of a grid-forming inverter based on sliding-mode and mixed H $_2$ /H ∞ control," *IEEE Transactions on Industrial Electronics*, vol. 64, no. 5, pp. 3862–3872, 2016.
- [43] P. Buduma and G. Panda, "Robust nested loop control scheme for lcl-filtered inverter-based dg unit in grid-connected and islanded modes," *IET Renewable Power Generation*, vol. 12, no. 11, pp. 1269–1285, 2018.
- [44] P. Kundur, N. Balu, and M. Lauby, *Power System Stability and Control*, ser. EPRI power system engineering. McGraw-Hill Education, 1994.
- [45] "IEEE standard for interconnection and interoperability of distributed energy resources with associated electric power systems interfaces–

- amendment 1: To provide more flexibility for adoption of abnormal operating performance category iii." *IEEE Std 1547a-2020 (Amendment to IEEE Std 1547-2018)*, pp. 1–16, 2020.
- [46] S. Skogestad and I. Postlethwaite, *Multivariable feedback control: analysis and design*. Citeseer, 2007, vol. 2.
 - [47] "IEEE recommended practice and requirements for harmonic control in electric power systems," *IEEE Std 519-2014 (Revision of IEEE Std 519-1992)*, pp. 1–29, June 2014.
 - [48] K. Strunz, R. H. Fletcher, R. Campbell, and F. Gao, "Developing benchmark models for low-voltage distribution feeders," in *2009 IEEE Power Energy Society General Meeting*, July 2009, pp. 1–3.
 - [49] G. F. Lauss, M. O. Faruque, K. Schoder, C. Dufour, A. Viehweider, and J. Langston, "Characteristics and design of power hardware-in-the-loop simulations for electrical power systems," *IEEE Transactions on Industrial Electronics*, vol. 63, no. 1, pp. 406–417, 2016.
 - [50] M. Ciobotaru, R. Teodorescu, and F. Blaabjerg, "A new single-phase pll structure based on second order generalized integrator," in *2006 37th IEEE Power Electronics Specialists Conference*. IEEE, 2006, pp. 1–6.
 - [51] M. C. Chandorkar, D. M. Divan, and R. Adapa, "Control of parallel connected inverters in standalone ac supply systems," *IEEE transactions on industry applications*, vol. 29, no. 1, pp. 136–143, 1993.